ELSEVIER

NeuroImage

www.elsevier.com/locate/ynimg
NeuroImage 40 (2008) 1064–1076

Studying the human brain anatomical network via diffusion-weighted MRI and Graph Theory

Yasser Iturria-Medina,[a,*] Roberto C. Sotero,[b] Erick J. Canales-Rodríguez,[a] Yasser Alemán-Gómez,[a] and Lester Melie-García[a]

[a]*Neuroimaging Department, Cuban Neuroscience Center, Avenue 25, Esq 158, #15202, PO Box 6412, Cubanacán, Playa, Havana, Cuba*
[b]*Brain Dynamics Department, Cuban Neuroscience Center, Havana, Cuba*

Received 20 June 2007; revised 18 October 2007; accepted 30 October 2007
Available online 19 November 2007

Our goal is to study the human brain anatomical network. For this, the anatomical connection probabilities (ACP) between 90 cortical and subcortical brain gray matter areas are estimated from diffusion-weighted Magnetic Resonance Imaging (DW-MRI) techniques. The ACP between any two areas gives the probability that those areas are connected at least by a single nervous fiber. Then, the brain is modeled as a non-directed weighted graph with continuous arc weights given by the ACP matrix. Based on this approach, complex networks properties such as small-world attributes, efficiency, degree distribution, vulnerability, betweenness centrality and motifs composition are studied. The analysis was carried out for 20 right-handed healthy subjects (mean age: 31.10, S.D.: 7.43). According to the results, all networks have small-world and broad-scale characteristics. Additionally, human brain anatomical networks present bigger local efficiency and smaller global efficiency than the corresponding random networks. In a vulnerability and betweenness centrality analysis, the most indispensable and critical anatomical areas were identified: putamens, precuneus, insulas, superior parietals and superior frontals. Interestingly, some areas have a negative vulnerability (e.g. superior temporal poles, pallidums, supramarginals and hechls), which suggest that even at the cost of losing in global anatomical efficiency, these structures were maintained through the evolutionary processes due to their important functions. Finally, symmetrical characteristic building blocks (motifs) of size 3 and 4 were calculated, obtaining that motifs of size 4 are the expanded version of motif of size 3. These results are in agreement with previous anatomical studies in the cat and macaque cerebral cortex.

Introduction

The brain is one of the most challenging systems found in nature. It can be viewed as a complex network consisting of highly interconnected processing regions. Its response to any external stimulus relies on the cooperation among these specialized centers, which can be classified according to their anatomical and functional properties (Brodmann, 1909; Mazziotta et al., 1995; Toga et al., 2006; Mountcastle, 2007). Thus, the study of their anatomical and functional connectivity constitutes an indispensable step towards the understanding of the brain specialization and integration (Sporns et al., 2005).

Previous works in mammalian species (i.e. cat and macaque monkey) have shown that cortical anatomical connection matrices, obtained post-mortem, exhibit "small-world" attributes (Sporns and Zwi, 2004; Hilgetag and Kaiser, 2004). That is, anatomical brain connection patterns are characterized by a high clustering index and a short average distance between any two regions. Small-world topology is generally associated with global and local parallel information processing, sparse connectivity between nodes and low wiring costs (Bassett and Bullmore, 2006). Using this same connectivity datasets, structural and functional motifs composition (characteristic network building blocks) were studied (Sporns and Kotter, 2004). The results supported the hypothesis that while brain networks maximize both the number and the diversity of functional motifs, the repertoire of structural motifs is relatively small.

Functional human brain networks derived from functional Magnetic Resonance Imaging (fMRI), Electroencephalogram (EEG) and Magnetoencephalographic (MEG) data also exhibit small-world properties (Stam, 2004; Eguiluz et al., 2005; Salvador et al., 2005; Achard et al., 2006; Bassett et al., 2006). However, characteristics of the human brain anatomical network have been poorly investigated. This is due to difficulties in defining the basic structural elements of the human brain in terms of nodes and connections (Sporns et al., 2005) and also because the common invasive tracer methods cannot be applied. Recent steps in that direction were given by He et al. (2007), which investigated anatomical connections patterns in the human cerebral cortex in vivo using cortical thickness measurements from magnetic resonance images. For this, the cerebral cortex was segmented into 54 different areas for 124 normal brains, and any two areas

* Corresponding author. Fax: +53 7 208 6707.
E-mail address: iturria@cneuro.edu.cu (Y. Iturria-Medina).
Available online on ScienceDirect (www.sciencedirect.com).

1053-8119/$ - see front matter © 2008 Published by Elsevier Inc.
doi:10.1016/j.neuroimage.2007.10.060

were considered anatomically connected if they had statistically significant correlations in cortical thickness. This is based on studies suggesting that interregional statistical associations in cortical thickness provide important connectivity information (Worsley et al., 2005; Lerch et al., 2006). Then, a threshold value was applied to interregional correlation matrix in order to construct a binary undirected graph and estimate its properties, principally small-world properties and the connectivity degree distribution. Their results supported the hypothesis that human brain anatomical networks present small-world attributes and follow a degree distribution characterized by an exponentially truncated power-law. However, as their approach was limited to cortical networks, important subcortical structures such as the thalamus or the amygdales, which keep vital connections with cortical areas, were not taken into account.

On the other hand, the development of diffusion-weighted Magnetic Resonance Imaging (DW-MRI) techniques in the last decade makes possible the noninvasive study of the anatomical circuitry of the living human brain (Mori et al., 1999; Conturo et al., 1999; Tuch, 2002; Parker et al., 2002; Koch et al., 2002; Behrens et al., 2003; Hagmann et al., 2006; Iturria-Medina et al., 2007). In this context, Hagmann et al. (2006) reported for the first time small-world attributes in networks of small human cortical areas estimated from DW-MRI techniques. In that study, nodes of the analyzed network corresponded to small cubic regions of interest (ROI) covering the gray matter tissue, while arc weights were assigned according to the estimated fiber densities between nodes, which had been previously computed using an in vivo probabilistic nervous fiber tracking procedure (Wedeen et al., 2005). By applying a threshold to the created graph, an unweighted version was constructed and its small-world and hierarchical properties were analyzed. Their results show similar small-world topologies to those obtained for the rat and macaque monkey brain networks, which were created using post-mortem tracing techniques.

In the present paper we continue the characterization of the human brain anatomical connections by extending previous works in several ways. First, instead of an unweighted graph as in Hagmann et al. (2006) and He et al. (2007), a weighted version will be used for modeling the brain anatomical network. In this approach, the weights are obtained from the anatomical connections probability (ACP) matrix which gives the probability that any two areas are connected at least by a single nervous fiber. For obtaining the ACP matrix, anatomical connections patterns between 90 different anatomical gray matter regions will be estimated using DW-MRI techniques and Graph Theory (Iturria-Medina et al., 2007). These regions include both cortical and subcortical structures as defined by Tzourio-Mazoyer et al. (2002) according to functional and anatomical criteria. Finally, in addition to previous small-world and degree distribution analysis, other important network properties, such as efficiency, vulnerability, betweenness centrality and motif composition will be investigated.

The remainder of the paper is organized as follows. In the Materials and methods section the DW-MRI methodology used for estimating brain anatomical connections is briefly described, and it is shown that the obtained anatomical network can be viewed as a weighted non-directed graph. After that, concepts like small-world and network efficiency, degree distribution, vulnerability, betweenness centrality and motifs composition are briefly exposed. The experimental data and its preprocessing are also described. In the Results section significant findings are presented. Finally, the last section summarizes and discusses the principal results, and proposes some open problems to be considered in future studies.

Materials and methods

Mapping zone-zone brain anatomical connections using DW-MRI

DW-MRI techniques have being widely used to estimate the nervous fiber pathways connecting brain regions of interest (Mori et al., 1999; Conturo et al., 1999; Tuch, 2002; Parker et al., 2002; Koch et al., 2002; Behrens et al., 2003; Hagmann et al., 2006; Iturria-Medina et al., 2007). Recently, a novel DW-MRI and Graph Theory methodology (Iturria-Medina et al., 2007) was introduced with the principal purpose of summarizing anatomical connections patterns between brain gray matter areas. The proposed procedure consists of three major steps:

1. The cerebral volume is represented as a non-directed weighted graph $G_{brain,0}=[N_0, A_0, W_0]$, where N_0 is the set of voxels (nodes) having a non-zero probability of belonging to some cerebral tissue, A_0 is the set of white matter links (arcs) between contiguous voxels in N_0, and W_0 is a set of real numbers representing arcs weights. The weight of an arc is chosen so that it represents the probability that contiguous linked nodes are really connected by nervous fibers. It is defined by taken into account both the probability that linked nodes belong to gray/white matter (evaluated according to the probabilistic tissues segmentation of the corresponding anatomic T1-weighted image) and the probability of nervous fibers to be oriented around the direction of the arc (evaluated using the intravoxel white matter Orientational Distribution Function [ODF] estimated via DW-MRI techniques) (see Eq. (A1)). This ensures that only those pairs of contiguous nodes with high probability of belonging to gray/white matter and high probability of sharing fibers will have high arc weights, which is equivalent to have high probability of being connected. Also, since the DW-MRI profile is symmetric (efferent and afferent projections can not be distinguished) $G_{brain,0}$ is modeled as a non-directed graph (i.e. distinction between initial and terminal arc nodes is irrelevant).
2. In this step, an iterative algorithm (see Appendix C) is employed for finding the most probable trajectory (see Eq. ((A6)) between any two nodes, which is assumed to be the hypothetical nervous fiber pathway running between these points. Thus, quantification of the anatomical connectivity between both points is carried out according to the intrinsic information of this estimated connection route. Specifically, the node-node anatomical connectivity measure (ranging between 0, not connected, and 1, perfectly connected) is defined as the lowest weight of the arcs set belonging to the most probable path (see Eq. (A7)). This ensures that only those brain points with high arc weights (probability of white matter connection) of all the arcs belonging to their connection route will have a high connectivity value.
3. In order to characterize anatomical connections between n brain gray matter structures, the previous graph $G_{brain,0}$ is redefined as a $n+1$ partite graph G_{brain} by partitioning the initial nodes set N_0 into n non-overlapped gray matter subsets and one subset clustering the remaining nodes. In this context, the new weighted non-directed brain graph $G_{brain}=[N, A, W]$ consist of a set N of n nodes (gray matter regions), a set A of arcs (direct white matter connections between gray matter regions) and a set W of arc

weights (probability of connections between the gray matter regions). Graphically, G_{brain} is a discrete set of points (nodes) representing anatomic regions and a set of lines without arrow (arcs) representing connections between the regions. Based on the latter, three connectivity measures were defined: Anatomical Connection Strength (ACS), Anatomical Connection Density (ACD) and Anatomical Connection Probability (ACP). The interpretation of these measures is as follows. ACS provides an estimation of the potential information flow between any pair of regions, which is considered proportional to the amount of nervous fibers shared by these regions. As an indicator of the latter, we took the cross section area of the fiber connector volume on the surfaces of the two regions. This is estimated by counting the "effective" number of nodes on the surfaces of the zones involved in the connection, where each node is counted according to its maximum probability of being connected with the nodes in the surface of the second zone (see Eq. (A8)). On the other hand, ACD is a measure of the fraction of the connected superficial nodes with respect to the total number of superficial nodes of both areas (see Eq. (A10)). It allows, for example, to know if a pair of zones has more or less connection density than other pair of zones with different or equal number of superficial nodes. Finally, ACP measures the maximum probability of any two regions to be connected at least by a single nervous fiber connection. It is estimated as the maximum connectivity value between the superficial nodes of both involved areas (see Eq. (A11)) and allows to infer if any two gray matter regions can be functionally related independently of the strength and density of their possible anatomical connection.

In the present study, as our goal is to analyze a map of possible brain anatomical connections implying potential functional interchange between gray matter areas (i.e. which areas are directly connected or not), we employ the ACP measure for weighting zone-zone connections in G_{brain}. Further works might include ACS and ACD measures in order to complement the description of the brain anatomical network.

Graph analysis to characterize brain anatomical connections

A great number of natural systems can be represented by complex networks. Graph Theory is usually considered the most appropriate framework for the mathematical treatment of complex networks. In general, a complex network can be represented as a graph in which nodes correspond to the elements of the system and arcs to the interactions between them (Boccaletti et al., 2006). In our specific case, we want to study the weighted brain network $G_{brain}=[N, A, W]$, which model the anatomical connections between 90 cortical and subcortical gray matter regions. G_{brain} will be characterized attending to six basic aspects: small-world, network efficiency, degree distribution, vulnerability, betweenness centrality and motifs composition.

Small-world and network efficiency

The concept of "small-world" is strongly related to the average shortest path length (L) and clustering coefficient (C) concepts. Let us explain these in detail: the average shortest path length (L) of a given graph $G=[N, A, W]$, is a measure of the typical separation between two nodes i and j ($\forall i, j \in N$), and it is defined as the mean of geodesic lengths d_{ij} over all pairs of nodes (Watts and Strogatz, 1998; Watts, 1999; Boccaletti et al., 2006):

$$L = \frac{1}{n(n-1)} \sum_{\substack{i,j \in G \\ i \neq j}} d_{ij} \tag{1}$$

In the unweighted network context ($w_{ij}=[0,1] \in \mathbb{N}$), the geodesic length d_{ij} is defined as the number of arcs along the shortest path connecting nodes i and j. In the case of weighted networks ($w_{ij} \in \mathbb{R}$), the path with the minimum number of nodes is not necessarily the optimal d_{ij} and in some cases it is necessary to define a physical length associated to each arc (this should be a function of the characteristics of the hypothetical link among any nodes i and j). In this work, we follow the suggestion of Boccaletti et al. (2006), and assume that the physical length of an arc connecting nodes i and j is inversely proportional to the probability of the analyzed connection, i.e. $l_{ij} = \frac{1}{w_{ij}}$. That is, as the probability of nervous fiber connection is lower the nodes are more distant. Note that this assumption do not penalizes arc length according to the real spatial separation between the position of the modeled gray matter regions or according to the longitude of the connecting fiber pathway. This is because the defined probability of nervous fiber connection only depends on the "diffusion data coherence" and the white/gray matter presence along the estimated connection routes, and not on its longitude. Thus, long range connections (such as those maintained by the optic radiation and the occipital–frontal fascicule) can have arc length values similar to short range connections, only depending of their corresponding connection probabilities. The geodesic length d_{ij} is finally defined as the smallest sum of the arc lengths throughout all the possible paths from node i to node j. Note that for the particular case of unweighted graphs, $l_{ij}=1$ for all arcs and the geodesic lengths d_{ij} reduces to the minimum number of arcs traversed to get from i to j.

On the other hand, the clustering coefficient is a measure of the inherent tendency to cluster nodes into strictly connected neighborhoods (Watts and Strogatz, 1998). In a weighted graph, the clustering around a node i can be calculated as the geometric average of subgraph node weights (Onnela et al., 2005):

$$C_i = \frac{1}{k_i(k_i-1)} \sum_{\substack{j,k \in G \\ j,k \neq i}} \left(\tilde{w}_{ij} \cdot \tilde{w}_{jk} \cdot \tilde{w}_{ki}\right)^{\frac{1}{3}}, \tag{2}$$

where k_i is the number of arcs connecting node i (named degree of the node i) and the weights are scaled by the largest weight in the network, $\tilde{w}_{ij} = \frac{w_{ij}}{\max(w_{ij})}$. The clustering coefficient for the whole graph G is defined as the average of clustering around each node (Watts and Strogatz, 1998):

$$C = \frac{1}{n} \sum_{i \in G} C_i. \tag{3}$$

Formally, Watts and Strogatz (1998) defined small-world networks as those having small average shortest path length, like random networks ($\lambda \equiv \frac{L^{real}}{L^{rand}} \sim 1$), and high clustering coefficient, much larger than random networks ($\gamma \equiv \frac{C^{real}}{C^{rand}} \gg 1$). Additionally, the small-worldness condition lies in satisfying that $\sigma \equiv \frac{\gamma}{\lambda} > 1$ (Humphries et al., 2006).

The concept of small-world has been also expressed in terms of the information flow (Latora and Marchiori, 2001). That is, small-world networks are very efficient in terms of global and local communication (they have high global and local efficiency E_{glob} and E_{loc}, respectively). The E_{glob} of a graph G is defined as:

$$E_{glob} = \frac{1}{n(n-1)} \sum_{\substack{i,j \in G \\ i \neq j}} \frac{1}{d_{ij}}. \quad (4)$$

This measure reflects how efficiently information can be exchanged over the network, considering a parallel system in which each node sends information concurrently along the network. On the other hand, the E_{loc} of G is defined as the average efficiency of the local subgraphs:

$$E_{loc} = \frac{1}{n} \sum_{i \in G} E_{glob}(G_i), \quad (5)$$

where G_i is the subgraph of the neighbors of i. This measure reveals how much the system is fault tolerant, showing how efficient the communication is among the first neighbors of i when it is removed. That is, the efficiency formalization gives a clear physical meaning to the concept of small-world, and allows a precise quantitative analysis of weighted networks (Latora and Marchiori, 2001).

In order to compare the efficiency of a given real network with the efficiency of its equivalent random network (characterized by the same number of nodes and arcs placed randomly), from now on we will refer to the relative local efficiency (E^*_{loc}) and the relative global efficiency (E^*_{glob}) measures (i.e. the ratio between the local and global efficiencies of the real and random networks respectively).

Degree distribution

Since not all nodes in a complex network have the same degree, usually a degree distribution $P(k)$ is defined. This gives the probability that a randomly selected node has k arcs (Erdös and Rényi, 1959). The degree distribution properties are commonly employed to classify networks into different categories. Amaral et al. (2000) presented evidences of the occurrence of three classes of small-world networks attending to their degree distribution properties: 1) scale-free networks, 2) broad-scale networks, and 3) single-scale networks.

Scale-free networks, for example the World-Wide Web (Albert et al., 1999), are characterized by a degree distribution that decays as a power law, i.e. $P(k) \sim k^{-\alpha}$, with exponents varying in the range $2 < \alpha < 3$. This power law indicates the preferential attachment of the nodes in the network to some specific hub nodes.

Broad-scale networks are characterized by a degree distribution that has a power law regime followed by a sharp cutoff, i.e. $P(k) \sim k^{\alpha-1} f(k/k_{crit})$. The function $f(k/k_{crit})$ has a sharp cut-off for degrees $k > k_{crit}$, constraining the number of nodes that can be connected to the hub nodes.

Finally, single-scale networks are characterized by a degree distribution with a fast decaying tail, i.e. $P(k) \sim f(k/k_{crit})$. Commonly for single-scale and broad-scale regime the sharp cutoff functions $f(k/k_{crit})$ are exponential or Gaussian (Amaral et al., 2000).

The information expressed by the degree distribution function is often presented by the cumulative degree distribution $P_c(k) = \sum_{k'=k}^{\infty} P(k')$, which is usually used to reduce the effects of noise corresponding to small networks (Strogatz, 2001; He et al., 2007).

Vulnerability

The vulnerability analysis of complex networks provides valuable quantitative information about the possible damage caused by the hypothetical failure of its elements. That is, this type of analysis allows to identify which are the most critical or indispensable structures for the appropriate operation of the network, and in the specific case of brain networks, it could be useful to evaluate the damage caused by illness known to affect gray matter connections such as Alzheimer Disease (Pearson et al., 1985; Morrison et al., 1986) and Schizophrenia (Mitelman et al., 2007).

By associating the performance of a network with its global efficiency, the vulnerability V_i of a node i can be defined as the drop in network performance when node i and its connections are removed (Newman and Park, 2003; Goldshtein et al., 2004; L.da F. Costa et al., 2006):

$$V_i = \frac{E_{glob} - E^i_{glob}}{E_{glob}}, \quad (6)$$

where E_{glob} and E^i_{glob} are the global efficiency of the network with and without node i.

Then, the vulnerability of the entire network G is defined as the maximum vulnerability for all of its nodes (Latora and Marchiori, 2005; L.da F.Costa et al., 2006):

$$V = \max_i V_i. \quad (7)$$

Betweenness centrality

Betweenness centrality is a widely used measure to identify the most central nodes in a graph, which are associated to those nodes that acts as bridges between the others nodes (Freeman, 1977; Dall'Asta et al., 2006; Bassett et al., 2006; Honey et al., 2007). It is defined as the fraction of shortest paths between pairs of nodes that passes through a given node. Mathematically, for weighted networks, if σ^w_{kj} is the total number of shortest paths from k to j and $\sigma^w_{kj}(i)$ is the number of these paths passing through node i, the weighted betweenness centrality of node i is (Dall'Asta et al., 2006):

$$b^w_i = \sum_{\substack{k,j \in G \\ k \neq j}} \frac{\sigma^w_{kj}(i)}{\sigma^w_{kj}}. \quad (8)$$

Motifs composition

Network motifs are subgraphs that appear more frequently in a real network than could be statistically expected, and are associated to the network evolution (Milos et al., 2002; Sporns and Kotter, 2004; Onnela et al., 2005). To detect those motifs that are likely to be important, Milos et al. (2002) proposed to compare the analyzed real network to suitably randomized networks and to select patterns appearing in the real network at numbers significantly higher than those in the randomized networks. Different motifs classes are

generally distinguished according to the motif's size (M), representing the number of involved nodes, and the number and pattern of interconnections.

In the case of weighted networks, Onnela et al. (2005) defined the *intensity* (I_M) of motif M as the geometric mean of its arc weights, and the *coherence* (Q_M) of motif M as the ratio of the geometric to the corresponding arithmetic mean. Based on these measures, motif scores were defined as:

$$ZI_M = \frac{(I_M - \langle i_M \rangle)}{\left(\langle i_M^2 \rangle - \langle i_M \rangle^2\right)^{\frac{1}{2}}},$$
$$ZQ_M = \frac{(Q_M - \langle q_M \rangle)}{\left(\langle q_M^2 \rangle - \langle q_M \rangle^2\right)^{\frac{1}{2}}}, \quad (9)$$

where ZI_M and ZQ_M are the motif intensity and coherence score respectively; i_M and q_M are the total intensity and coherence of motif M in one realization of the random regime, respectively.

Experimental data

DW-MRI datasets corresponding to 20 right-handed healthy subjects (mean age: 31.10, S.D.: 7.43) were acquired using a MRI scanner Siemens Symphony 1.5 T (Erlangen, Germany) and a single shot EPI sequence. Each dataset consists of 12 diffusion-weighted images and a $b=0$ image, with the following parameters: 50 contiguous slices of 3 mm thickness; $b=1200$ s/mm^2 for the weighted images; FOV=256×256 mm^2; acquisition matrix=128×128; corresponding to an 'in plane' spatial resolution of 2×2 mm^2; TE/TR=160 ms/7000 ms. The aforementioned acquisition was repeated 5 times to improve signal to noise ratio (SNR). In order to improve EPI quality, magnitude and phase difference images of a T2 gradient echo field mapping sequence were acquired with TE=7.71 ms and 12.47 ms. Also, for each subject a 3D high resolution T1-weighted image (MPRAGE) covering the whole brain was acquired with the following parameters: 160 contiguous slices of 1 mm thickness in sagittal orientation; in plane FOV=256×256 mm^2, corresponding to an in plane spatial resolution of 1×1 mm^2; TE/TR=3.93 ms/3000 ms.

In order to remove remaining distortions an affine 3D mutual normalized information-based registration method (Studholme et al., 1998) was used. The DW-MRI images were corrected from EPI distortions using the SPM FieldMap toolbox (Hutton et al., 2002). The T1-weighted 3D anatomical image was registered to the $b=0$ image using a normalized mutual information method (Studholme et al., 1998). Both diffusion-weighted images and T1-weighted images were interpolated and written with a spatial resolution of 2×2×2 mm^3. The registered interpolated T1-weighted image was automatically segmented into 90 gray matter structures (Tzourio-Mazoyer et al., 2002) using the IBASPM toolbox (available at http://www.fil.ion.ucl.ac.uk/spm/ext/#23IBASPM) (Alemán-Gómez et al., 2006). ODF maps were estimated using the procedure described in Appendix B.

Additionally, a set of three brain anatomical connectivity matrices were obtained from the Computational Cognitive Neuroscience Laboratory, Indiana University Bloomington (http://www.indiana.edu/~cortex/CCNL.html). These datasets correspond to the cat cerebral cortex, the macaque monkey visual cortex and the macaque monkey cerebral cortex, and consist of unweighted matrices with number of nodes 95, 30 and 73, respectively.

In all cases, randomized counterpart versions of the original networks were created using a rewiring algorithm (Maslov and Sneppen, 2002). This algorithm preserves the degree of each individual node, but connection weights are randomized until weight correlations with the original network are lost.

Results

Fiber tracking and zone–zone connectivity

Using the DW-MRI methodology described above, anatomical connections between the defined 90 brain gray matter structures were estimated for the 20 healthy subjects. Fig. 1 presents the obtained mean intersubject ACP matrix. The element C_{ij} is the connectivity value between regions i and j. As previously mentioned, this map is symmetric. Self connections are excluded, which implies a diagonal black line in the matrix. Also, it should be kept in mind that for each subject the anatomical reconstruction consisted of the whole brain with the two hemispheres (i.e. including callosal connections). Note for example the high connectivity values between the left and right superior frontal gyrus, or between the left and right superior occipital poles, which is in accordance with existing anatomical knowledge (Gómez-Padrón et al., 1985; Witelson, 1989; Standring, 2004).

In order to evaluate intersubject dis(similarity), correlations coefficients between their corresponding ACP matrices were calculated. Significant correlations coefficients were obtained (ranging between 0.65 and 0.88) with corresponding p values in the order of 10^{-220}.

Small-world and network efficiency analysis

First, the relative clustering coefficient γ, the relative average shortest path length λ and the small-worldness parameter σ were calculated for each subject. The results (first three columns of Table 1) confirm the expected small-world attributes of the studied brain anatomical networks according to the Watts-Strogatz (1998) and Humphries et al. (2006) conditions (i.e. $\lambda \sim 1$, $\gamma \gg 1$ and $\sigma > 1$). The obtained mean parameters of interest were $\gamma_{mean}=1.85$, $\lambda_{mean}=1.12$ and $\sigma_{mean}=1.64$, satisfying the previous conditions.

In a second statistical analysis, a network efficiency study revealed that, compared with the corresponding random networks, the human brain architectural network (as well as other mammalian species brain networks, as we will see later) presents smaller global efficiency and bigger local efficiency, i.e. both individual and mean values of E^*_{glob} are under 1, while the corresponding E^*_{loc} values are always above 1 (see columns 4 and 5 of Table 1, respectively). These results are in accordance with those obtained for brain functional networks corresponding to the same gray matter parcellation scheme (Achard and Bullmore, 2007). In the Summary and discussion section we will comment more about this, including the analysis of other mammalian brain species results.

Degree distribution analysis

A degree distribution analysis revealed that the studied brain anatomical networks correspond to a power law regime followed by a sharp cutoff, as broad-scale networks. Table 1 (columns 6 and 7) presents the obtained α and k_{crit} parameters corresponding to a broad-scale regime following the form $P(k) \sim k^{\alpha-1} \exp(k/k_{crit})$.

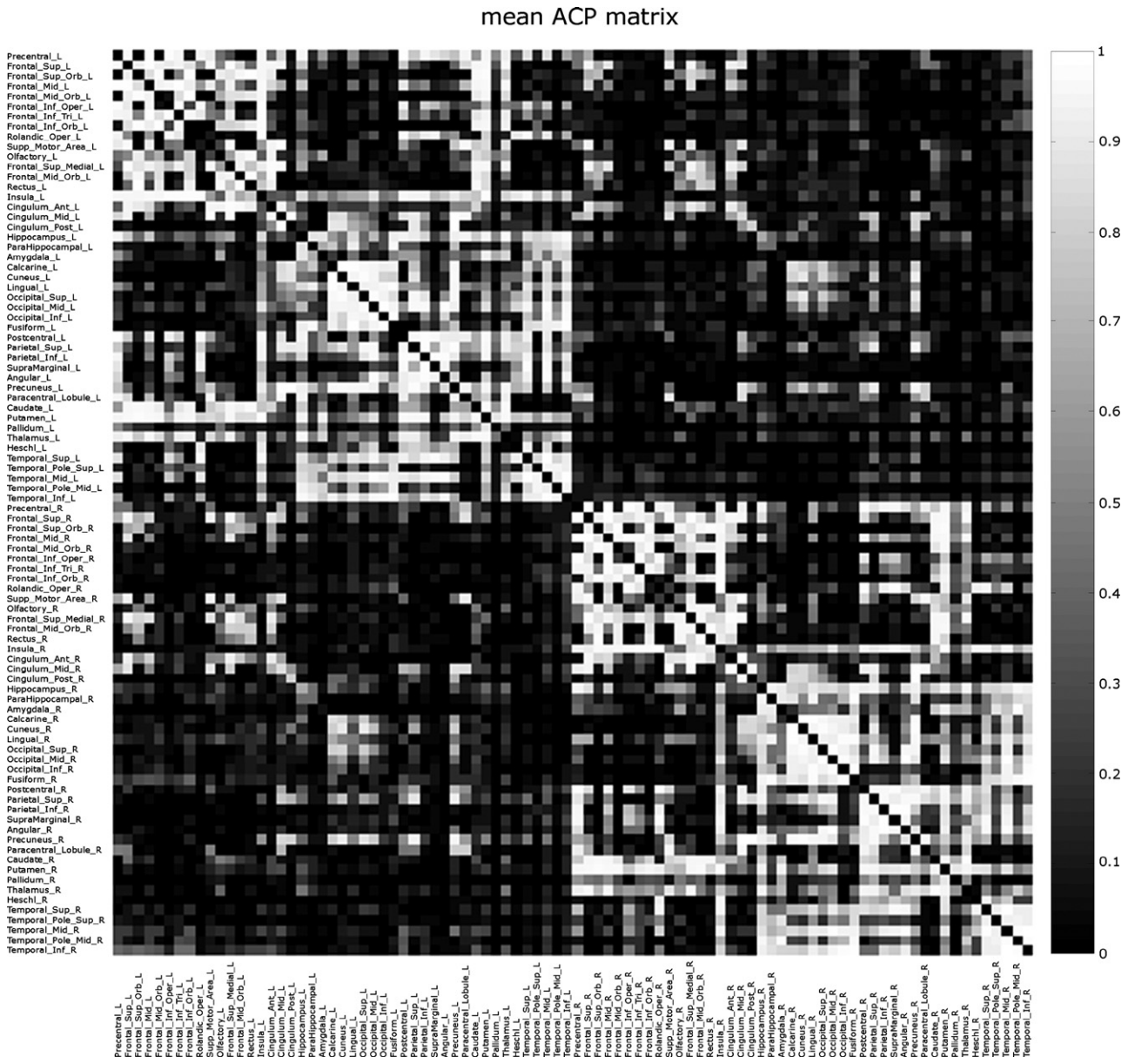

Fig. 1. Mean ACP matrix for 90 gray matter regions defined on the brain of 20 healthy subjects. The element $C_{i,j}$ is the connectivity value between regions i and j. Self connections are excluded, which implies a diagonal black line in the matrix. As previously mentioned, this map is symmetric. The color code represents the index of connectivity.

Fig. 2 illustrates the inter-subject mean cumulative degree distribution and its standard deviation. All the corresponding multiple determination coefficients, R-square (i.e. a measure of how successful the fit is in explaining the variation of the data, a value closer to 1 indicates a better fit), were in the order of 0.99. The mean estimated exponent α was 1.34. Additionally, the resulting mean parameter k_{crit} indicate that even the most connected areas in the brain have a physical constraint of around 5.81 inter-regional connections according to the used gray matter parcellation. These results are similar to those reported in Achard et al. (2006) for a human functional network involving the same gray matter areas (i.e. a degree distribution followed an exponentially truncated power law with an exponent parameter $\alpha=1.80$ and a cutoff degree $k_{crit}=5$).

Vulnerability and betweenness centrality analysis

In order to make a first inference about the most critical or indispensable structures in the brain anatomical networks, the vulnerability of the 90 defined brain gray matter areas for each subject were computed using expression (6). Fig. 3a summarizes the obtained mean vulnerability results. The identified most vulnerable areas are: putamens, precuneus, insulas, superior parietals and superior frontals. In a complementary analysis, the betweenness centrality of each gray matter area was estimated using expression (8). The identified most central areas agree totally with the obtained in the previous vulnerability analysis (see Fig. 3b). In both cases, the selected regions were identified by applying a z-test (H_0: $z=0$) with a 0.05 significance level to the resulting

Table 1
Obtained human brain networks attributes

Subjects	γ	λ	σ	E^*_{glob}	E^*_{loc}	α	k_{crit}
1	1.65	1.11	1.48	0.94	1.15	1.38	6.49
2	1.52	1.10	1.37	0.94	1.11	1.33	6.11
3	1.64	1.12	1.46	0.93	1.14	1.36	6.13
4	1.83	1.13	1.62	0.92	1.24	1.37	5.72
5	1.67	1.12	1.48	0.93	1.19	1.40	5.85
6	2.00	1.13	1.77	0.92	1.28	1.36	5.72
7	1.69	1.11	1.52	0.93	1.17	1.52	6.62
8	1.92	1.12	1.71	0.93	1.32	1.28	5.35
9	1.51	1.08	1.39	0.95	1.13	1.40	6.47
10	2.37	1.16	2.04	0.90	1.42	1.28	5.34
11	1.77	1.12	1.57	0.93	1.17	1.31	5.52
12	2.19	1.15	1.90	0.91	1.37	1.33	5.50
13	1.61	1.11	1.44	0.93	1.18	1.30	5.86
14	2.13	1.14	1.86	0.92	1.31	1.38	6.01
15	1.83	1.13	1.61	0.92	1.25	1.33	5.59
16	1.91	1.13	1.67	0.92	1.24	1.31	5.65
17	2.05	1.14	1.79	0.92	1.27	1.29	5.43
18	1.87	1.13	1.64	0.92	1.23	1.30	5.32
19	1.73	1.11	1.56	0.93	1.19	1.28	5.78
20	2.11	1.16	1.81	0.91	1.36	1.32	5.81
Mean	1.85	1.12	1.64	0.93	1.24	1.34	5.81
S.D.	0.23	0.02	0.18	0.01	0.08	0.05	0.38

mean vulnerability and mean betweenness centrality vectors respectively.

Motifs composition

Since the human brain anatomical networks studied here are symmetrical, our motifs composition analysis was restricted to find only those symmetrical motifs that appear significantly increased in the analyzed networks (let us say motifs with identity number [ID] 9 and 13 for motifs of size 3, and motifs with ID 75, 95, 159, 178, 194 and 199 for motifs of size 4; see Fig. 4a). In order to carry out the motifs analysis, 30 reference random matrices were generated. Fig. 4b and c show the obtained motifs intensity and motifs coherence scores for each subject, with motifs sizes 3 and 4, respectively. Notice that for $M=3$ (Fig. 4b), only a candidate motif with ID=13 seems to appear significantly increased while for $M=4$ (Fig. 4c) candidate motifs with ID=159, 194 and 199 are those that seem to appear significantly increased. Using a 0.05 significance level, we confirmed that the mentioned candidate motifs show statistically significant intensity and coherence deviation from the reference system, being them the obtained symmetrical human brain motifs of size 3 and 4.

Summary and discussion

In this work some basic statistical aspects of the human brain anatomical network were analyzed. The studied networks consisted of white matter connections between 90 cortical and subcortical gray matter regions, which were defined according to functional and anatomical criterions (Tzourio-Mazoyer et al., 2002). Connections among the different regions were estimated for 20 healthy subjects according to a graph-based DW-MRI procedure (Iturria-Medina et al., 2007) and the weighted networks analysis was centered in their small-world attributes, efficiency, degree distribution, vulnerability, betweenness centrality and motifs composition properties.

To our knowledge, until now only two previous works have being presented with a similar purpose. In the first previous study (Hagmann et al., 2006), the analyzed brain network consisted of a lot of gray matter cubic regions defining nodes whose corresponding arc weights connections were assigned according to the estimated nervous fiber density (Hagmann et al., 2004) between them. An unweighted version of the created graph was analyzed taking into account its small-world and hierarchical properties. In the second previous study (He et al., 2007), the network summarized the obtained connectivity patterns between 54 cortical areas segmented for 124 normal brains. Connections between areas were estimated using cortical thickness measurements from magnetic resonance images. The brain anatomical unweighted network analysis was centered principally in its small-world attributes and degree distribution properties.

In our first brain anatomical network statistical analysis, small-world and efficiency properties were studied. The results confirm the small-world attributes of the human brain anatomical network (Table 1). The obtained mean parameters of interest were $\gamma_{mean}=1.85$, $\lambda_{mean}=1.12$, with a resulting small-worldness parameter of $\sigma_{mean}=1.64$, satisfying the Watts-Strogatz (1998) and Humphries et al. (2006) conditions (i.e. $\lambda\sim1$, $\gamma\gg1$ and $\sigma>1$). However, it is important to notice that according to Hagmann et al. (2006), small-worldness parameter as well as the relative clustering coefficient should increases significantly when the number of brain network nodes increases. Although our results are in agreement with the results reported by Hagmann et al. (2006) and He et al. (2007) it should be noted that the used gray matter parcellation procedures differ in these studies. Additionally, our analysis was based on a weighted network scheme in contrast to an unweighted scheme as in previous works. Unfortunately, these procedure differences hinder a reliable quantitative parameter comparison between these three human anatomical studies.

Other brain mammalian species (cat and macaque monkey) present similar small-world anatomical attributes (Sporns and Zwi, 2004; Hilgetag and Kaiser, 2004). Nevertheless, as happens with previous human studies, a quantitative parameters comparison between our results and the reported by these post-mortem tracing animal studies it is not straightforward due to differences in the employed procedures (mainly the different used gray matter segmentation schemes).

In addition, the network efficiency analysis provided an interesting result: compared with the corresponding random networks, human brain anatomical networks present bigger local efficiency and smaller global efficiency. These results agree with that obtained by Achard and Bullmore (2007) for human brain functional networks, and also with those obtained by us for the cat cerebral cortex ($E^*_{loc}=1.37$ and $E^*_{glob}=0.96$), the macaque monkey visual cortex ($E^*_{loc}=1.24$ and $E^*_{glob}=0.97$) and the macaque monkey cerebral cortex ($E^*_{loc}=1.86$ and $E^*_{glob}=0.93$). In our opinion, this suggests that mammalian brains evolved trying to maintain a high local efficiency, which is equivalent to prioritize the integration among regions specialized in similar types of functional information and, also, guaranties the tolerance to possible fails at the local level. On the other hand, the global efficiency (i.e. the capacity to exchange information among all the regions) is small compared with corresponding random networks. A reason for this could be that the global exchange may not be completely necessary, a fact related to the optimization of the brain integration process.

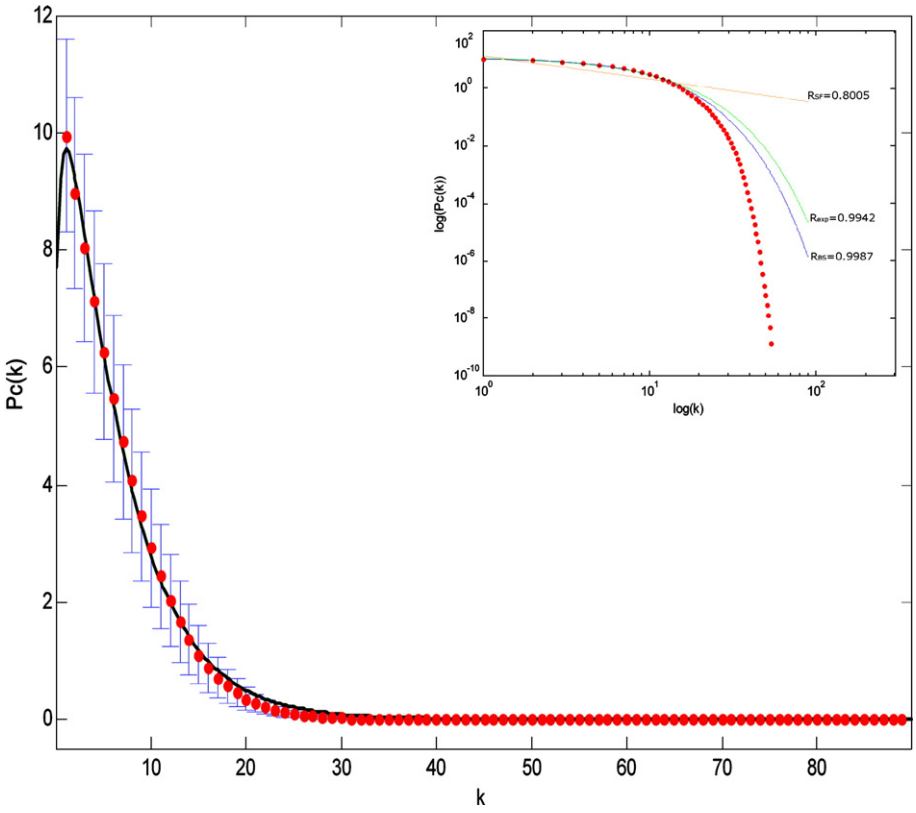

Fig. 2. Estimated inter-subject mean cumulative degree distribution (red points) and standard deviation (blue error bars). The green line represents the fitted exponential truncated power law corresponding to a broad scale regime of the form $P(k) \sim k^{\alpha-1}\exp(k/k_{crit})$, with $\alpha=1.34$ and $k_{crit}=5.81$. Inset: log–log plot of the mean cumulative degree distribution. The red points indicate observed data, the blue line is the best fitted exponential truncated power law ($R_{BS}=0.9987$), the green line is an exponential ($R_{exp}=0.9942$), and the orange line is a power law ($R_{SF}=0.8005$).

A degree distribution analysis revealed that the studied brain networks present a power-law regime followed by a sharp cutoff (Fig. 2), as broad-scale networks. In this kind of networks, the preferential attachment to the hub nodes has a physical constraint, which in terms of brain anatomical connections is related to the maximum number of areas connected to the hub nodes and responds to structural cost optimization process (e.g. optimization of the axonal volume covering inter-regional brain connections). In addition, other anatomical and functional human brain studies have presented similar degree distribution results (Achard et al., 2006; He et al., 2007). This supports the broad-scale attributes of the human brain network; however, final conclusions about this topic require future analysis to much larger brain networks with thousands of nodes.

The vulnerability and betweenness centrality analysis allowed identifying the most critical anatomical nodes in the brain, reveling quantitative information about the global damage caused by the hypothetical failure of these nodes. According to the gray matter parcellation that was used, the most vulnerable and central areas were (see Fig. 3): putamens, precuneus, insulas, superior parietals and superior frontals. On the other hand, note that some areas cause a negative vulnerability to the studied brain networks, which means that the anatomical brain system can be more efficient without them (the most representative are: superior temporal poles, pallidums, supramarginals and hechls). This can be related to the anatomical cost of their existence, and suggest that even implying a possible loss in global anatomical efficiency, these structures were maintained in the brain circuitry through the evolutionary processes due to their specific important functions. Also, as an interesting point, we may have expected that thalamic regions belong to the most critical or indispensable gray matter centers in the brain. However, the used vulnerability and betweenness centrality measures are strongly related to the number of connections of the analyzed areas, and the obtained results indicate that thalamic regions are not the most connected areas although surely they have important connections with some specific anatomic regions.

In the context of brain networks, a structural (anatomical) motif may consist of a set of brain areas and pathways that can be potentially engage in different patterns of interactions (Sporns and Kotter, 2004). In practice, networks motifs are identified as those subgraphs appearing more frequently in a real network than could be statically expected (Milos et al., 2002; Onnela et al., 2005). In this work, it was looked for the first time into the structural motif composition of the human brain anatomical network. According to the used gray matter parcellation and the employed weighted motif detection procedures (Onnela et al., 2005), the obtained structural motifs were those with ID=13, for $M=3$, and with ID=159, 194 and 199, for $M=4$ (see Fig. 4). This result keeps some essential similarities with the obtained for cat and macaque cerebral cortex by Sporns and Kotter (2004), that is: motifs at $M=4$ are the expanded versions of the obtained motif at $M=3$, forming a reciprocally connected nodes chain, where pairs of connections linking the ends of the chain can be absent; thus, nodes in the

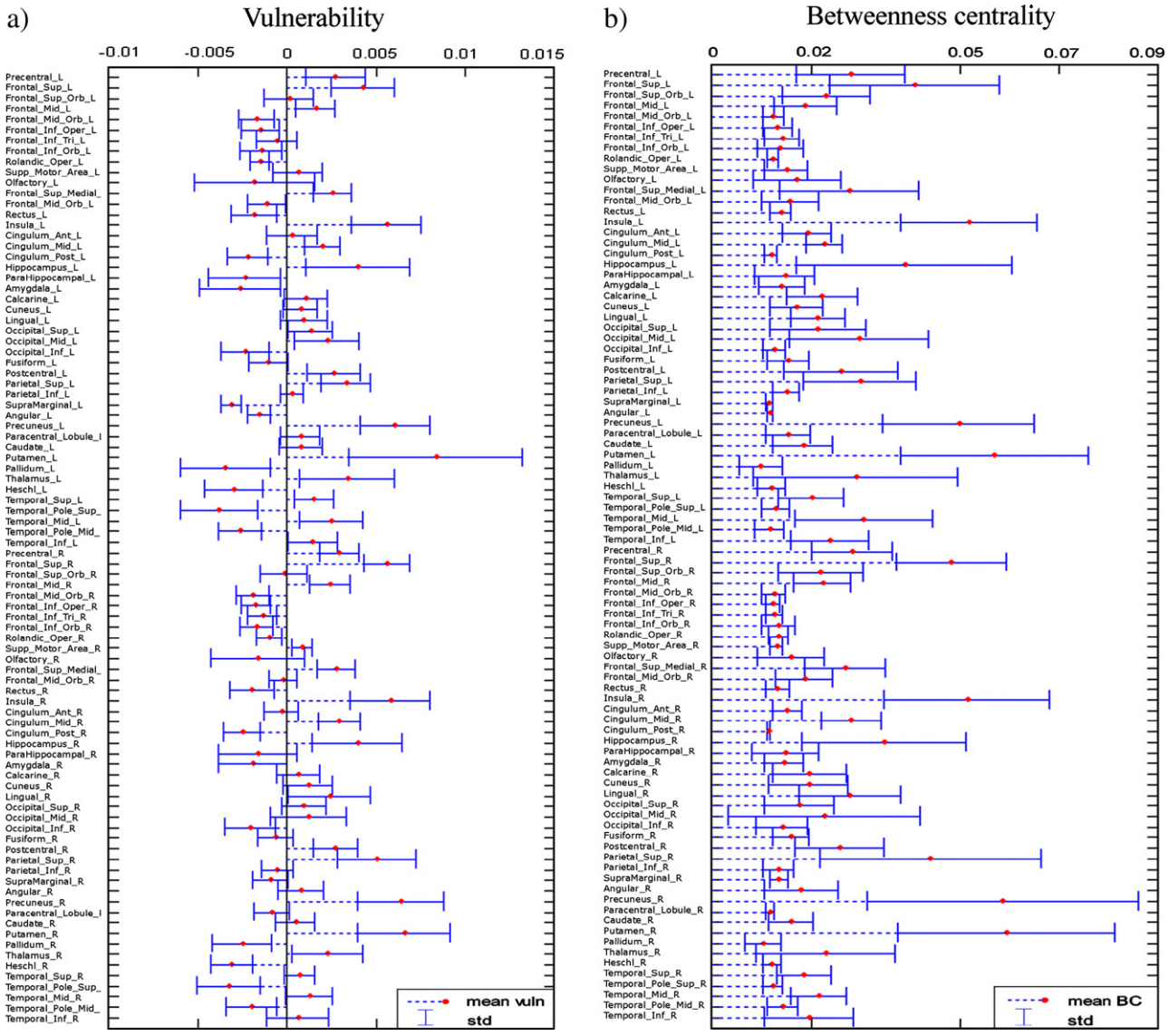

Fig. 3. Mean inter-subject vulnerability (a) and betweennes centrality (b) results for the 90 defined brain gray matter areas. Additionally, using a z-test (H_0: $z=0$) with a 0.05 significance level, the most vulnerable and central areas were identified. In both cases, these areas are: putamens, precuneus, insulas, superior parietals, and superior frontals.

motifs are highly integrated with their neighbors although some of them do not communicate directly, reflecting the basic principles of integration and segregation in the brain.

A limitation of the presented study is the symmetrical configuration of the analyzed brain connectivity matrices, which is a consequence of the inherent symmetrical properties of DW-MRI techniques (distinction between afferent and efferent fiber projections it is not possible yet). This fact causes, for example, the restriction of the motif composition analysis to consider only those symmetrical candidate motifs. Nevertheless, a previous work (Young, 1993) reported that around 85% of the total possible connections between 73 primate brain areas are reciprocals.

An important element in the DW-MRI Graph-Based methodology employed here for estimating brain anatomical connections (Iturria-Medina et al., 2007) is the angular resolution of the diffusion-weighted images. In this work we used low angular resolution data due to a system limitation, but certainly more reliable results can be obtained using high angular resolution techniques, which allows a more precise characterization of the intravoxel white matter orientation (Tuch, 2004; Wedeen et al., 2005) and thus a more realistic characterization of the brain structure. Other relevant matter is how to use the obtained ACP matrices to elucidate which gray matter areas are actually connected or not. A tentative alternative could be the selection of a threshold value to create unweighted connectivity matrices. However, the choice of the appropriate threshold is generally an elusive point, and that's why in this study we chose to work only with probability of connections between zones instead of the simpler on–off connectivity analysis. Additionally, future works might be directed to explore the effects of different tracking methods on the network attributes. Surely, common findings across different tracking methods would provide more confidence for the anatomical network graphical description. Nonetheless, in recent studies (unconcluded) we have obtained significant similarity

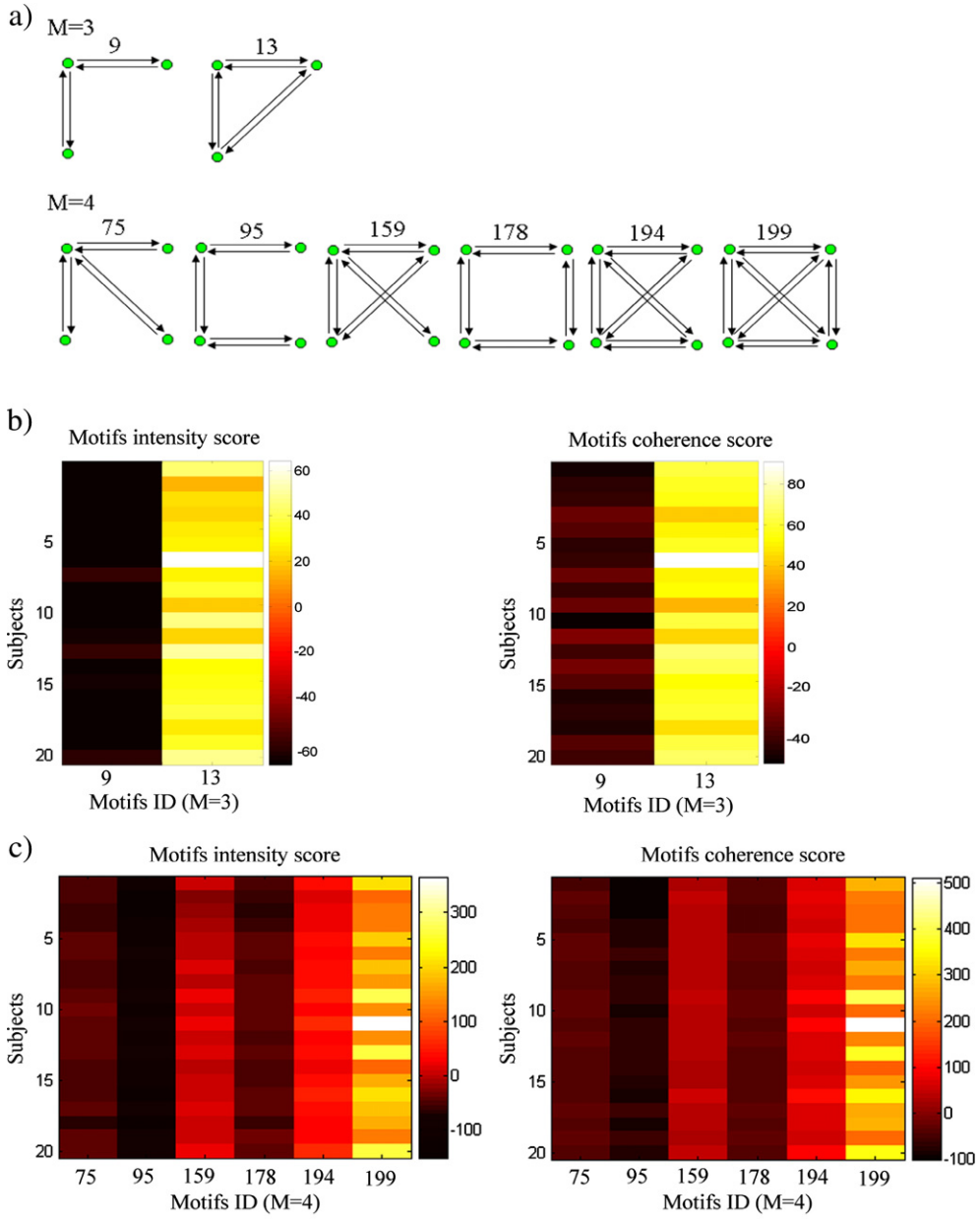

Fig. 4. Motifs results for motifs size $M=3$ and $M=4$. (a) Candidate symmetrical motifs of size 3 and 4. Numbers refer to the motif's identity number (ID). (b) Obtained motifs intensity and motifs coherence scores for each subject, with $M=3$. (c) Obtained motifs intensity and motifs coherence scores for each subject, with $M=4$. In panels (b) and (c), the color code represents the z-score index. Using a 0.05 significance level, significant motifs found in the analyzed human brain networks were those with ID=13, for $M=3$, and with ID=159, 194 and 199, for $M=4$.

among the connectivity patterns of healthy subjects using two different fiber tractography procedures (i.e. the Graph-based method employed here and the probabilistic tracking method implemented in the FSL software package [http://www.fmrib.ox.ac.uk/fsl]). This will be the subject of a separate publication.

Reliable gray matter parcellation is crucial for obtaining consistent connectivity patterns between individuals. Therefore, a key element of the used methodology to create the brain anatomical network is its high dependency on the employed atlas. Although the atlas used here was carefully created taking into account relevant anatomical and functional details (Tzourio-Mazoyer et al., 2002), in the future it might be more meaningful to use advanced integrative atlases based on finer cytoarchitecture, myeloarchitecture and MRI procedures (Toga et al., 2006; He et al., 2007).

Further studies should focus on: improving the characterization of the brain anatomical connections (using for example high angular resolution DW-MRI techniques, a priori connectivity information and others fiber tracking methodologies), extending the analysis to other interesting network properties (such as brain complexity, hierarchical features and functional motif composition) and to other brain connection measures (such as ACS and ACD), as well as exploring sex and right–left handed (dis)similarities.

Appendix A. Mathematical expressions of the used DW-MRI and Graph-based connectivity model

Arc weights

Given the weighted non-directed graph $G_{\text{brain},0}=[N_0,\ A_0,\ W_0]$, the weight of an arc $a_{ij}\in A_0$ linking two contiguous nodes i and j ($i,j\in N_0$), with spatial vectors position $\overrightarrow{r_i}$ and $\overrightarrow{r_j}$ respectively, is defined as:

$$w(a_{ij})\equiv w(a_{ji}) = P_{\text{mat}}(\overrightarrow{r_i})P_{\text{mat}}(\overrightarrow{r_j})[P_{\text{diff}}(\overrightarrow{r_i},\Delta\overrightarrow{r_{ij}}) + P_{\text{diff}}(\overrightarrow{r_j},\Delta\overrightarrow{r_{ji}})], \tag{A1}$$

where the two basics functions P_{mat} and P_{diff} enclose anatomical and diffusion information respectively. The first of these functions was defined as follows:

$$P_{\text{mat}}(\overrightarrow{r}) = \frac{\alpha P_{\text{WM}}(\overrightarrow{r}) + P_{\text{GM}}(\overrightarrow{r})}{1+(\alpha-1)P_{\text{WM}}(\overrightarrow{r})}, \tag{A2}$$

where P_{WM} and P_{GM} are probabilistic maps of white and gray matter (WM and GM) respectively and α is a tuning parameter.

The other function, $P_{\text{diff}}(\overrightarrow{r_i},\Delta\overrightarrow{r_{ij}})$, characterizes fiber coherence along $\Delta\overrightarrow{r_{ij}} = \overrightarrow{r_j} - \overrightarrow{r_i}$, which is the direction of the arc a_{ij}, and can be inferred from DW-MRI images using methods for the description of the intravoxel white matter structure. Here, $P_{\text{diff}}(\overrightarrow{r_i},\Delta\overrightarrow{r_{ij}})$ is assumed to be the integral of the fiber Orientational Distribution Function (ODF) over a solid angle β around $\Delta\overrightarrow{r_{ij}}$:

$$P_{\text{diff}}(\overrightarrow{r_i},\Delta\overrightarrow{r_{ij}}) = \frac{1}{Z}\int_{\beta}\text{ODF}(\overrightarrow{r_i},\Delta\overrightarrow{r_{ij}})\text{d}S. \tag{A3}$$

Z is a normalization constant chosen to fix to 0.5 the maximum value of the set $\{P_{\text{diff}}(\overrightarrow{r_i},\Delta\overrightarrow{r_{ij}})\}_{\forall\overrightarrow{r_j}\in N_i^{\text{neig}}}$. Note that generally $P_{\text{diff}}(\overrightarrow{r_i},\Delta\overrightarrow{r_{ij}})\neq P_{\text{diff}}(\overrightarrow{r_j},\Delta\overrightarrow{r_{ji}})$.

Fiber tracking and node–node connectivity

In the previous graph $G_{\text{brain},0}$, where each arc weight is considered as the probability of its existence, the problem of searching the most probable path between nodes $\overrightarrow{r_{i_1}}$ and $\overrightarrow{r_{i_L}}$ is equivalent to find the path $\rho_{i_1\ldots i_L}=\{a_{i_1i_2};a_{i_2i_3};\ldots;a_{i_{L-1}i_L}\}$ with maximum total probability:

$$P[\rho_{i_1\ldots i_L}] = w(a_{i_1,i_2})\prod_{k=2}^{L-1}w^{\text{cond}}(a_{i_ki_{k+1}}|a_{i_{k-1}i_k})\Psi(\rho_{i_{k-1}\ldots i_{k+1}}), \tag{A4}$$

where the term $w^{cond}(a_{i_ki_{k+1}}|a_{i_{k-1}i_k})$ is the conditional weight of the arc $a_{i_ki_{k+1}}$ given arc $a_{i_{k-1}i_k}$:

$$w^{\text{cond}}(a_{i_ki_{k+1}}|a_{i_{k-1}i_k}) = P_{\text{mat}}(\overrightarrow{r_{i_{k+1}}})[P_{\text{diff}}(\overrightarrow{r_{i_k}},\Delta\overrightarrow{r_{i_ki_{k+1}}}) + P_{\text{diff}}(\overrightarrow{r_{i_{k+1}}},\Delta\overrightarrow{r_{i_{k+1}i_k}})]. \tag{A5}$$

The function Ψ penalizes path curvature between any three consecutive steps of the path and is selected in a way that allows only those fiber trajectories with curvature angles smaller than 90°.

Based on this, the estimated nervous fiber trajectory running from $\overrightarrow{r_{i_1}}$ and $\overrightarrow{r_{i_L}}$ will be given by the most probable path:

$$\tilde{\rho}_{i_1\ldots i_L} = \underset{\forall\rho_{i_1\ldots i_L}}{\text{argmax}}(P[\rho_{i_1\ldots i_L}]). \tag{A6}$$

To solve previous Eq. (A6) an iterative algorithm was proposed (see Appendix C). Then, quantification of the anatomical connectivity between nodes $\overrightarrow{r_{i_1}}$ and $\overrightarrow{r_{i_L}}$ is defined according to the parameters of the connection route among them, specifically as the lowest weight of the arcs belonging to it:

$$C_{\text{node}}(\overrightarrow{r_{i_1}},\overrightarrow{r_{i_L}}) = \min_{\forall a\in\tilde{\rho}_{i_1\ldots i_L}}(w(a)). \tag{A7}$$

Zone–zone connectivity

The expression for the ACS measure between any two gray matter regions R_1 and R_2 reads:

$$C_{\text{Zone}}^{\text{ACS}}(R_1,R_2) = \sum_{\forall\overrightarrow{r_m}\in N_2^s}\zeta_{\overrightarrow{r_m}} + \sum_{\forall\overrightarrow{r_n}\in N_1^s}\zeta_{\overrightarrow{r_n}}, \tag{A8}$$

where the term $\zeta_{\overrightarrow{r_n}}(0\leq\zeta_{\overrightarrow{r_n}}\leq 1)$ denotes the connectivity value of a node $\overrightarrow{r_n}\in N_1^s$ (being N_1^s the set of superficial nodes of R_1) with R_2. It is defined as the maximum node–node connectivity value (see Eq. (A7)) among all connections between $\overrightarrow{r_n}$ and any $\overrightarrow{r_m}\in N_2^s$ (being N_2^s the set of superficial nodes of R_2):

$$\zeta_{\overrightarrow{r_n}} = \max_{\forall\overrightarrow{r_m}\in N_2^s}(C_{\text{node}}(\overrightarrow{r_n},\overrightarrow{r_m})). \tag{A9}$$

Similarly, $\zeta_{\overrightarrow{r_m}}$ denotes the connectivity of any node $\overrightarrow{r_m}\in N_2^s$ with R_1. Note that the first term of expression (A8) quantifies connections of the region R_2 with R_1, and the second term quantifies connections of the region R_1 with R_2.

ACD measure is estimated as the ACS relative to the number of nodes belonging to the surfaces of R_1 and R_2:

$$C_{\text{Zone}}^{\text{ACD}}(R_1,R_2) = \frac{C_{\text{Zone}}^{\text{ACS}}(R_1,R_2)}{|N_1^s|+|N_2^s|}. \tag{A10}$$

ACP represents the probability of regions R_1 and R_2 to be connected at least by a single fiber connection. It is estimated as the maximum connectivity value between nodes of these regions:

$$C_{\text{Zone}}^{\text{ACP}}(r_1,r_2) = \max\left(\max_{\forall\overrightarrow{r_m}\in N_2^s}\zeta_{\overrightarrow{r_m}},\max_{\forall\overrightarrow{r_n}\in N_1^s}\zeta_{\overrightarrow{r_n}}\right). \tag{A11}$$

Appendix B. White matter Orientational Distribution Function

The intravoxel white matter orientational distribution function (ODF) $\psi(\hat{u})$ is defined as the radial projection of the probability density function (PDF) $P(\overrightarrow{R})$ (Wedeen et al., 2005):

$$\psi(\hat{u}) = \int_0^{+\infty}R^2P(\hat{u}R)\text{d}R, \tag{B1}$$

being $\hat{u}$ a unitary vector and $\overrightarrow{R}=\hat{u}R$ the relative spin displacement.

Considering the PDF for anisotropic Gaussian diffusion:

$$P\left(\overrightarrow{R}\right) = (4\pi t)^{-3/2}(|\mathbf{D}|)^{-1/2}\text{e}^{\frac{-\overrightarrow{R}^T\mathbf{D}^{-1}\overrightarrow{R}}{4t}}, \tag{B2}$$

Then, substituting in Eq. (B1) and using the identity:

$$\int_0^{+\infty}x^m\text{e}^{ax^2}\text{d}x = \frac{\Gamma\left(\frac{(m+1)}{2}\right)}{2a^{\frac{m+1}{2}}}, \tag{B3}$$

where Γ is the Gamma function, we can obtain the ODF as:

$$\psi(\hat{u}) = \frac{1}{C}\left(\hat{u}^T\mathbf{D}^{-1}\hat{u}\right)^{-\frac{3}{2}}. \tag{B4}$$

Here, C is a normalization constant which ensures that the ODF is properly normalized to unit mass.

Appendix C. Algorithm to solve the most probable path problem

Given a Brain Graph $G_{\text{brain},0}=[N_0, A_0, W_0]$, let us define some quantities before setting up the algorithm:

$|N_0|$: Cardinality of the set N_0, i.e. the number of elements belonging to set N_0.
N_0^{-s}: Set of nodes that belong to $G_{\text{brain},0}$ except node 's', $N_0^{-s} = N_0/\{\overrightarrow{r_s}\}$.
$\mathrm{M}(\overrightarrow{r_v})$: Map of probabilities of the path between node 's' and all nodes $\overrightarrow{r_v}\in N_0^{-s}, \mathrm{M}(\overrightarrow{r_v}) = P[\rho(\overrightarrow{r_s}, \overrightarrow{r_v})]$ and $\mathrm{M}(\overrightarrow{r_s})=1$.
N_i^{neig}: Nearest neighborhood of the ith node.

This algorithm proceeds in $|N_0|-1$ iterations as follows:

a) Set initially:
$a.1)$ $\tilde{S}=N_0^{-s}$,
$a.2)$ $\mathrm{M}(\overrightarrow{r_i}) = \begin{cases} 1, & \overrightarrow{r_i}=\overrightarrow{r_s}, \\ w_0(a_{si}), & \overrightarrow{r_i}\in N_i^{\text{neig}} \\ 0, & \text{otherwise.} \end{cases}$
$a.3)$ $\tilde{\rho}(\overrightarrow{r_s}, \overrightarrow{r_i}) = a_{si}, \quad \forall \overrightarrow{r_i}\in N_s^{\text{neig}}$
b) Find $\overrightarrow{r_j}\in \tilde{S}$ such that $\mathrm{M}(\overrightarrow{r_j}) = \max_{\forall r_i\in\tilde{S}} \mathrm{M}(\overrightarrow{r_i})$
b.1) Set a new $\tilde{S}\leftarrow\tilde{S}/\{\overrightarrow{r_j}\}$
b.2) If $\tilde{S}=\varnothing$, then Stop; else continue
c) For all $\overrightarrow{r_m}\in N_j^{\text{neig}}$ and $\overrightarrow{r_m}\in S$, set
c.1) $\rho(\overrightarrow{r_s}, \overrightarrow{r_m}) = \{\tilde{\rho}(\overrightarrow{r_s}, \overrightarrow{r_j}) \cup a_{jm}\}$,
c.2) If $P[\rho(\overrightarrow{r_s}, \overrightarrow{r_m})]>\mathrm{M}(\overrightarrow{r_m})$ then
$\tilde{\rho}(\overrightarrow{r_s}, \overrightarrow{r_m})= \rho(\overrightarrow{r_s}, \overrightarrow{r_m}), \quad \mathrm{M}(\overrightarrow{r_m})= P[\tilde{\rho}(\overrightarrow{r_s}, \overrightarrow{r_m})]$
c.3) go to b).

Finally, the map $\mathrm{M}(\overrightarrow{r_p})$ for $\overrightarrow{r_p}\in N_0^{-s}$ represents the final probability of the path of maximum reliability according to (A6) between nodes $\overrightarrow{r_s}$ and $\overrightarrow{r_p}$ denoted by $\rho(\overrightarrow{r_s}, \overrightarrow{r_p})$.

References

Achard, S., Bullmore, E., 2007. Efficiency and cost of economical brain functional networks. PLoS Comput. Biol. 3 (2), e17 (Feb. 2).

Achard, S., Salvador, R., Whitcher, B., Suckling, J., Bullmore, E., 2006. A resilient, low-frequency, small-world human brain functional network with highly connected association cortical hubs. J. Neurosci. 26, 63–72.

Albert, R., Jeong, H., Barabasi, A.-L., 1999. Diameter World-Wide Web 130–131.

Alemán-Gómez, Y., Melie-García, L., Valdes-Hernández, P., 2006. IBASPM: Toolbox for automatic parcellation of brain structures. Presented at the 12th Annual Meeting of the Organization for Human Brain Mapping, June 11–15, 2006, Florence, Italy. Available on CD-Rom in NeuroImage, Vol. 27, No. 1.

Amaral, L.A., Scala, A., Barthelemy, M., Stanley, H.E., 2000. Classes of small-world networks. Proc. Natl. Acad. Sci. U. S. A. 97, 11149–11152.

Bassett, D.S., Bullmore, E., 2006. Small-world brain networks. Neuroscientist 12, 512–523.

Bassett, D.S., Meyer-Lindenberg, A., Achard, S., Duke, T., Bullmore, E., 2006. Adaptive reconfiguration of fractal small-world human brain functional networks 1. Proc. Natl. Acad. Sci. U. S. A. 103, 19518–19523.

Behrens, T.E., Johansen-Berg, H., Woolrich, M.W., Smith, S.M., Wheeler-Kingshott, C.A., Boulby, P.A., Barker, G.J., Sillery, E.L., Sheehan, K., Ciccarelli, O., Thompson, A.J., Brady, J.M., Matthews, P.M., 2003. Non-invasive mapping of connections between human thalamus and cortex using diffusion imaging. Nat. Neurosci. 6, 750–757.

Boccaletti, S., Latora, V., Moreno, Y., Chavez, M., Hwang, D.-U., 2006. Complex networks: structure and dynamics. Phys. Rep. 424, 175–308.

Brodmann, K., 1909. Vergleichende Lokalisationslehre der Grosshirnrinde in ihren Prinzipien dargestellt auf Grund des Zellenbaues, Barth, Leipzig. Thomas, Springfield, IL, 1960, pp. 201–230.

Conturo, T.E., Lori, N.F., Cull, T.S., Akbudak, E., Snyder, A.Z., Shimony, J.S., McKinstry, R.C., Burton, H., Raichle, M.E., 1999. Tracking neuronal fiber pathways in the living human brain. Proc. Natl. Acad. Sci. U. S. A. 96, 10422–10427.

Dall'Asta, L., Barrat, A., Barthelemy, M., Vespignani, A., 2006. Vulnerability of Weighted Networks. Dynamically Evolving, Large-scale Information Systems, TR-0340.

Eguiluz, V.M., Chialvo, D.R., Cecchi, G.A., Baliki, M., Apkarian, A.V., 2005. Scale-free brain functional networks. Phys. Rev. Lett. 94 (018102).

Erdös, P., Rényi, A., 1959. On random graphs. Publ. Math. Debrecen 6, 290.

Freeman, L., 1977. A set of measures of centrality based upon betweenness. Sociometry 40, 35–41.

Goldshtein, V., Koganov, G.A., Surdutovich, G.I., 2004. Vulnerability and Hierarchy of Complex Networks. Cond-mat/0409298.

Gómez-Padrón, I., Silva Loynaz, C., Seuc Chiu, A., 1985. Anatomía II. Folleto complementario. Ministerio de salud publica, Cuba.

Hagmann, P., Reese, T.G., Tseng, W.Y., Meuli, R., Thiran, J.P., Wedeen, V.J., 2004. Diffusion Spectrum Imaging tractography in complex cerebral white matter: aninvestigation of the centrum semiovale. Proc. ISMRM 623.

Hagmann, P., Kurant, M., Gigandet, X., Thiran, P., Wedeen, V.J., Meuli, R., Thiran, J.P., 2006. Imaging the brain neuronal network with diffusion MRI: a way to understand its global architecture. Proc. ISMRM 436.

He, Y., Chen, Z.J., Evans, A.C., 2007. Small-world anatomical networks in the human brain revealed by cortical thickness from MRI. Cereb. Cortex, doi:10.1093/cercor/bhl149.

Hilgetag, C.C., Kaiser, M., 2004. Clustered Organization of Cortical Connectivity, pp. 353–360 (2nd ed.).

Honey, C.J., Kotter, R., Breakspear, M., Sporns, O., 2007. Network structure of cerebral cortex shapes functional connectivity on multiple time scales. Proc. Natl. Acad. Sci. U.S.A. 104, 10240–10245.

Humphries, M.D., Gurney, K., Prescott, T.J., 2006. The brain stem reticular formation is a small-world, not scale-free, network. Proc. Biol. Sci. 273, 503–511.

Hutton, C., Bork, A., Josephs, O., Deichmann, R., Ashburner, J., Turner, R., 2002. Image distortion correction in fMRI: aquantitative evaluation. NeuroImage 16, 217–240.

Iturria-Medina, Y., Canales-Rodríguez, E.J., Melie-García, L., Valdes-Hernández, P.A., Martínez-Montes, E., Alemán-Gómez, Y., Sánchez-Bornot, J.M., 2007. Characterizing brain anatomical connections using diffusion weighted MRI and Graph Theory. NeuroImage 36, 645–660.

Koch, M.A., Norris, D.G., Hund-Georgiadis, M., 2002. An investigation of functional and anatomical connectivity using magnetic resonance imaging. NeuroImage 16, 241–250.

L. da F. Costa, Rodrigues, F.A., Travieso, G., Villas, P.R., 2006. Characterization of Complex Networks: A Survey of Measurements. (arXiv:cond-mat/0505185v5).

Latora, V., Marchiori, M., 2001. Efficient behavior of small-world networks5. Phys. Rev. Lett. 87 (198701).

Latora, V., Marchiori, M., 2005. Vulnerability and protection of infrastructure networks. Phys. Rev., EStat. Nonlinear Soft Matter Phys. 71 (1Pt2) (Jan; 015103).

Lerch, J.P., Worsley, K., Shaw, W.P., Greenstein, D.K., Lenroot, R.K., Giedd, J., Evans, A.C., 2006. Mapping anatomical correlations across cerebral cortex (MACACC) using cortical thickness from MRI. NeuroImage 31, 993–1003.

Maslov, S., Sneppen, K., 2002. Specificity and stability in topology of protein networks. Science 296 (5569), 910–913 (May 3).

Mazziotta, J.C., Toga, A.W., Evans, A., Fox, P., Lancaster, J., 1995. A probabilistic atlas of the human brain: theory and rationale for its development. The International Consortium for Brain Mapping (ICBM). NeuroImage 2, 89–101.

Milos, R., Shen-Orr, S., Itzkovitz, S., Kashan, N., Chklovskii, D., Alon, U., 2002. Network motifs: simple building blocks of complex networks. Science 298, 824–827.

Mitelman, S.A., Brickman, A.M., Shihabuddin, L., Newmark, R.E., Hazlett, E.A., Haznedar, M.M., Buchsbaum, M.S., 2007. A Comprehensive Assessment of Gray and White Matter Volumes and their Relationship to Outcome and Severity in Schizophrenia, doi:10.1016/j.neuroimage.2007.04.070.

Mori, S., Crain, B.J., Chacko, V.P., vanZijl, P.C., 1999. Three-dimensional tracking of axonal projections in the brain by magnetic resonance imaging. Ann. Neurol. 45, 265–269.

Morrison, J.H., Scherr, S., Lewis, D.A., Campbell, M.J., Bloom, F.E., 1986. The laminar and regional distribution of neocortical somatostatin and neuritic plaques: implications for Alzheimer's disease as a global neocortical disconnection syndrome. In: Scheibel, A.B., Weschler, A.F. (Eds.), The Biological Substrates of Alzheimer's Disease. Academic-Press, New York, NY, pp. 115–131.

Mountcastle, V.B., 2007. Perceptual Neuroscience: The Cerebral Cortex. Harvard University Press, Cambridge, MA.

Newman, M.E.J., Park, J., 2003. Why social networks are different from other types of networks. Phys. Rev., E 68 (036122).

Onnela, J.P., Saramaki, J., Kertesz, J., Kaski, K., 2005. Intensity and coherence of motifs in weighted complex networks. Phys. Rev., E Stat. Nonlinear Soft Matter Phys. 71 (065103).

Parker, G.J., Wheeler-Kingshott, C.A., Barker, G.J., 2002. Estimating distributed anatomical connectivity using fast marching methods and diffusion tensor imaging. IEEE Trans. Med. Imag. 21, 505–512.

Pearson, R.C.A., Esiri, M.M., Hiorns, R.W., Wilcock, G.K., Powell, T.P.S., 1985. Anatomical correlates of the distribution of the pathological changes in the neocortex in Alzheimer's disease. Proc. Natl. Acad. Sci. U.S.A. 82, 4531–4534.

Salvador, R., Suckling, J., Coleman, M.R., Pickard, J.D., Menon, D., Bullmore, E., 2005. Neurophysiological architecture of functional magnetic resonance images of human brain. Cereb. Cortex 15, 1332–1342.

Sporns, O., Kotter, R., 2004. Motifs in brain networks. PLoS. Biol. 2, e369.

Sporns, O., Zwi, J., 2004. The small world of the cerebral cortex. Neuroinformatics 2, 145–162.

Sporns, O., Tononi, G., Kotter, R., 2005. The human connectome: a structural description of the human brain. PLoS. Comput. Biol. 1, e42.

Stam, C.J., 2004. Functional connectivity patterns of human magnetoencephalographic recordings: a 'small-world' network? Neurosci. Lett. 355, 25–28.

Standring, S., 2004. Gray′s Anatomy: The Anatomical Basis of Medicine and Surgery, 39th edition. Churchill Livingstone.

Strogatz, S.H., 2001. Exploring complex networks. Nature 410 (6825), 268–276 (Mar 8).

Studholme, Hill, Hawkes, 1998. A normalized entropy measure of 3-D medical alignment. Proc. Medical Imaging, vol. 3338. SPIEPress, San Diego, CA, pp. 132–143.

Toga, A., Thompson, P., Susumu, M., Amunts, K., Zilles, K., 2006. Towards multi modal atlases of the human brain. Nat. Rev., Neurosci. 7 (12), 952–966.

Tuch, D.S., 2002. MRI of complex tissues tructure. PhD Thesis.

Tuch, D.S., 2004. Q-ballimaging. Magn. Reson. Med. 52, 1358–1372.

Tzourio-Mazoyer, N., Papathanassiou, D., Crivello, F., Etard, O., Delcroix, N., Mayozer, B., Joliot, M., 2002. Automated Anatomical Labeling of Activations in SPM Using a Macroscopic Anatomical Parcellation of the MNI MRI Single-Subject Brain, pp. 273–289 (15ed).

Watts, D.J., 1999. Small Worlds: The Dynamics of Networks between Order and Randomness. Princeton University Press, Princeton, NJ.

Watts, D.J., Strogatz, S.H., 1998. Collective Dynamics of Small-World Networks, pp. 440–442.

Wedeen, V.J., Hagmann, P., Tseng, W.Y., Reese, T.G., Weisskoff, R.M., 2005. Mapping complex tissue architecture with diffusion spectrum-magnetic resonance imaging. Magn. Reson. Med. 54, 1377–1386.

Witelson, S.F., 1989. Hand and sex differences in the isthmus and genu of the human corpuscallosum. A post mortem morphological study. Brain 112 (Pt3), 799–835.

Worsley, K.J., Chen, J.I., Lerch, J., Evans, A.C., 2005. Comparing functional connectivity via thresholding correlations and singular value decomposition. Philos. Trans. R. Soc. Lond., BBiol. Sci. 360, 913–920.

Young, M.P., 1993. The organization of neural systems in the primate cerebral cortex. Proc. Biol. Sci. 252, 13–18.